LANGMUIR
Article
Cite This: Langmuir 2018, 34, 6645−6652
pubs.acs.org/Langmuir

Inhibiting Reductive Elimination as an Intramolecular Disulfide Dramatically Enhances the Thermal Stability of SAMs on Gold Derived from Bidentate Adsorbents

Supachai Rittikulsittichai,[†,§] Chul Soon Park,[†,§] Maria D. Marquez,[†] Andrew C. Jamison,[†] Thomas Frank,[†] Chia-Hua Wu,[‡] Judy I. Wu,[‡] and T. Randall Lee*[,†]

[†]Department of Chemistry and the Texas Center for Superconductivity and [‡]Department of Chemistry, University of Houston, 4800 Calhoun Road, Houston, Texas 77204-5003, United States

Supporting Information

ABSTRACT: The bidentate aromatic adsorbate, 5-(octadecyloxy)-1,3-benzenedimethanethiol (**R1ArmDT**), with a specific design of extended S−S distance and a geometric constraint to resist cyclic disulfide formation was synthesized. The film formation and thermal stability of self-assembled monolayers (SAMs) derived from **R1ArmDT** were investigated and compared to those of SAMs derived from an analogous bidentate dithiol 2-(4-(octadecyloxy)-phenyl)-propane-1,3-dithiol (**R1ArDT**), in which the two sulfur atoms can readily form a cyclic disulfide upon reductive elimination from the surface. Although the SAMs derived from **R1ArmDT** were less densely packed than those derived from **R1ArDT**, as judged by the data obtained by X-ray photoelectron spectroscopy and polarization modulation infrared reflection absorption spectroscopy, the SAMs derived from **R1ArmDT** were markedly more thermally stable than those derived from **R1ArDT**. The greater thermal stability of the **R1ArmDT** SAMs can be rationalized on the basis of the structure of the bidentate **R1ArmDT** headgroup, in which the two pendant sulfur atoms cannot access each other intramolecularly to form a cyclic disulfide upon reductive elimination from the surface.

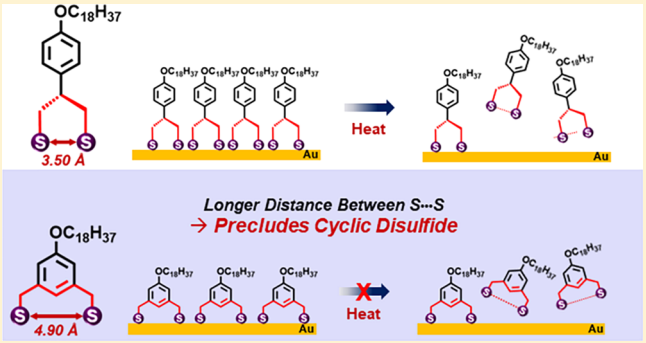

INTRODUCTION

The process of forming self-assembled monolayers (SAMs), a spontaneous self-molecular organization and assembly of organic molecules to form monolayer films, has been studied and developed as a widely used technique to control the interfacial properties of various substrates (e.g., metals, oxide surfaces, and inorganic semiconductors),[1,2] enabling their use in emerging applications involving biomaterial,[3−5] lithographic patterning,[6,7] and microelectronic device fabrication.[8,9] Additionally, these nanometric organic coatings when applied onto metal substrates are beneficial in protecting the metal surfaces against corrosion[10,11] and wear in tribological applications.[12] To develop and utilize these organic monolayer films for device fabrication and other practical applications, their thermal[13] and chemical stabilities[14,15] including their tolerance for lithographic conditions (i.e., UV light and electron beam)[16,17] are fundamental requirements. Although SAMs derived from *n*-alkanethiols on gold offer highly ordered and densely packed films, their stability is insufficient for use under a plethora of conditions; in particular, they decompose upon exposure to the atmosphere[18] and at elevated temperatures.[19,20] Several studies have found that the decomposition of *n*-alkanethiol-based SAMs involves the desorption of adsorbate molecules from the surface through the formation of intermolecular disulfides and/or oxidized thiolate species (i.e., thiosulfonate and thiosulfite).[21,22]

To improve the durability and stability of these films, several strategies have been employed to resist the desorption of adsorbate molecules induced by physical and chemical stimuli; these strategies include intermolecular hydrogen bondings,[19] underpotential metal depositions,[23] cross-linkage between neighboring adsorbates,[24] and multiple sulfur−gold interactions.[25−30] As for the latter case, the binding of sulfur to gold provides a bond enthalpy of ∼40−45 kcal/mol,[2] which is significantly stronger than van der Waals and hydrogen-bonding interactions. Furthermore, the entropy change for the loss of multidentate ligands is thermodynamically greater than that for monodentate ligands, a phenomenon known as the "chelate effect".[28−31] Notably, the use of custom-designed multidentate thiol headgroups can inhibit intramolecular cyclic disulfide formation during the desorption process.[13,28−30,32] Thus, appropriately designed multidentate thiols as adsorbates

Received: November 20, 2017
Revised: March 30, 2018
Published: May 9, 2018

DOI: 10.1021/acs.langmuir.7b03973
Langmuir 2018, 34, 6645−6652

on gold offer a viable strategy for generating monolayer films with enhanced stability.

Our research team recently examined the use of the aromatic dithiolate-based adsorbates, such as 2-(4-(octadecyloxy)-phenyl)propane-1,3-dithiol (**R1ArDT**) (see Figure 1), in efforts

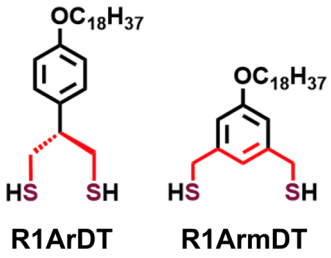

Figure 1. Structure of bidentate adsorbates compared in this study: **R1ArDT**[33] and 5-(octadecyloxy)-1,3-benzenedimethanethiol (**R1ArmDT**).

to generate monolayer films with enhanced stability.[33] The studies found that the thermal stability of SAMs derived from these adsorbates was enhanced by a combination of $\pi-\pi$ interactions between the aromatic rings and the chelate effect, which inhibits desorption due to ring strain of the resultant cyclic disulfide and alternatively requires the formation of entropically disfavored dimers (bis-disulfides), trimers (tris-disulfides), or even larger heterocycles.[33] Because the distance between sulfur atoms in multidentate headgroups is key to the generation of stable SAMs on gold,[25] we have continued to develop alternative bidentate aromatic adsorbates having intramolecular S−S distances and geometrical constraints that inhibit cyclic disulfide formation.

In the present study, we designed the structurally distinct bidentate aromatic adsorbate, 5-(octadecyloxy)-1,3-benzenedimethanethiol (**R1ArmDT**), in which the headgroup possesses a 1,3-benzodimethylmethane (1,3-BDMT) architecture (as shown in Figure 1). Notably, the sulfur atoms in the 1,3-BDMT architecture cannot combine to form an intramolecular cyclic disulfide. Although a handful of studies have used the 1,3-BDMT headgroup architecture to form SAMs on gold, none has provided an in-depth examination of the thermal stability of these types of SAMs.[28,29,33,34] Our investigation compares the structure and thermal stability of SAMs generated from **R1ArmDT**, bidentate **R1ArDT**, and monodentate octadecanethiol (**C18SH**) as a standard; for all three adsorbates, the length of the tailgroup consists of 18 carbon atoms.

EXPERIMENTAL SECTION

Synthesis of R1ArmDT and R1ArDT. A detailed description of the synthetic procedures used to prepare **R1ArmDT** (Scheme S1) and the corresponding ^{1}H and ^{13}C NMR spectra (Figures S1 and S2) are provided in the Supporting Information. We prepared **R1ArDT** as described in a previous report.[33]

Formation and Characterization of SAMs. Detailed descriptions of the procedures used to prepare and characterize the monolayers derived from **R1ArDT**, **R1ArmDT**, and **C18SH** are provided in the Supporting Information.

Evaluation of the Thermal Stability of SAMs at Elevated Temperature. The SAMs formed from **R1ArmDT**, **R1ArDT**, and **C18SH** on gold substrates were heated in isooctane at 80 °C and evaluated as a function of time. The gold slides were removed from solution at selected intervals of time and rinsed with toluene, tetrahydrofuran (THF), methanol, ethanol, and dried with ultrapure nitrogen. The samples were immediately characterized by ellipsometry and polarization modulation infrared reflection absorption spectroscopy (PM-IRRAS) and then reimmersed in the heating solvent. The relative ellipsometric thicknesses were used to determine the fraction of SAMs remaining on the gold surface.[28−30]

RESULTS AND DISCUSSION

Ellipsometric Thickness. Ellipsometry is a useful tool for providing a rapid and reliable evaluation of the molecular coverage of SAMs on gold. To analyze the relationship between the film thickness and the molecular orientation and packing density for the **R1ArmDT** SAMs, we constructed two different molecular models of **R1ArmDT**, in which the orientation of the benzene ring was aligned perpendicular and parallel relative to the surface normal, as shown in Figure S3. In these rudimentary models, we assumed for simplicity that the alkyl chains have a fully-trans-extended conformation and tilt ∼30° from the surface normal, as in SAMs on gold derived from *n*-alkanethiols.[35] Notably, the alkyl chains in a loosely packed monolayer exhibit a large average chain tilt from the surface normal due to the distance between chains induced by the relatively large aromatic headgroups, which can diminish chain−chain van der Waals interactions.[36,37] Consequently, loosely packed SAMs can be expected to exhibit a lower ellipsometric thickness when compared to that for their densely packed analogs.[36,37]

Table 1. Estimated Thicknesses and Measured Thicknesses for SAMs Generated from C18SH, R1ArDT, and R1ArmDT with a Flat and an Upright Orientation of the Benzene Ring for R1ArmDT in THF

adsorbate	calculated thickness (Å)	measured thickness (Å)
C18SH	22[19]	21.7 ± 0.8
R1ArDT	31	19.1 ± 0.3[33]
R1ArmDT (upright)	29	18.3 ± 0.4
R1ArmDT (flat)	27	

Table 1 compares the measured ellipsometric thicknesses of the monolayers derived from **R1ArDT** and **R1ArmDT** along with the theoretical thicknesses estimated from the aforementioned models; we also provide the ellipsometric constants to indicate the quality of the underlying gold substrates (Table S1). The relationships between thicknesses and molecular conformations of the **R1ArDT** SAMs have been described previously.[33] Specifically, the **R1ArDT** SAMs exhibited low film thicknesses that were lower than the theoretical thicknesses; the discrepancy was rationalized on the basis of a relatively large chain tilt and/or chain deformation to obtain low-energy conformations on the surface of gold.[33] Similarly, the ellipsometric thickness measured here for the **R1ArmDT** SAMs is significantly lower than the theoretical thickness determined from the molecular models of **R1ArmDT**. This latter discrepancy suggests chain disordering with a substantial chain tilt and low packing density of the alkyl chains in the **R1ArmDT** SAMs, which can be attributed to incommensurability in the size of the relatively large aromatic dithiolate headgroups and the smaller alkyl tailgroups. Unfortunately, the large difference in the calculated versus the experimental thicknesses precluded a determination of the orientation of the benzene ring in these SAMs from the ellipsometric data alone. Regrettably, efforts to obtain the orientation using polarization modulation infrared reflection absorption spectroscopy (PM-IRRAS) were also unsuccessful (vide infra).

DOI: 10.1021/acs.langmuir.7b03973
Langmuir 2018, 34, 6645−6652

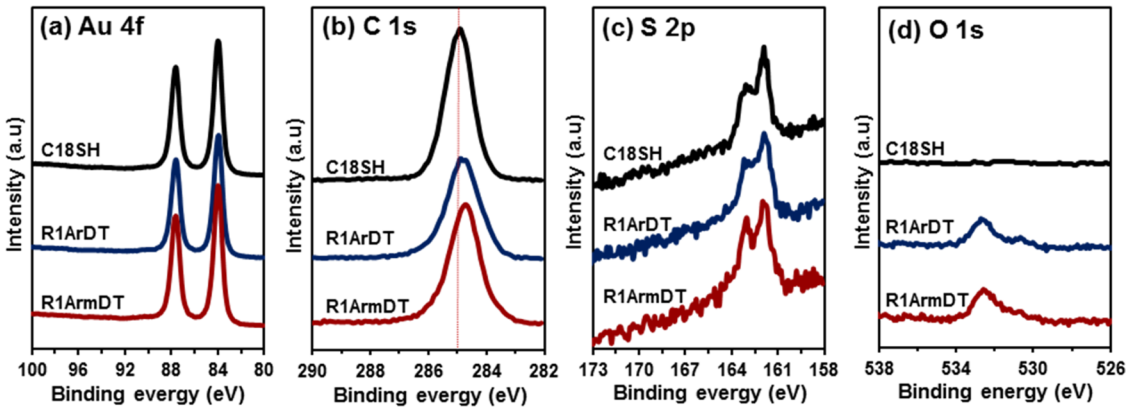

Figure 2. XP spectra of the (a) Au 4f, (b) C 1s, (c) S 2p, and (d) O 1s regions for SAMs formed from **C18SH**, **R1ArDT**, and **R1ArmDT** in THF.

Table 2. Relative Packing Densities of SAMs Formed from C18SH, R1ArDT, and R1ArmDT Determined by XPS from the S/Au Values

	S/Au			
adsorbate	sample 1	sample 2	sample 3	relative packing density (%)[a]
C18SH	0.054	0.053	0.056	100
R1ArDT	0.060	0.064	0.062	57 ± 2.8
R1ArmDT	0.052	0.058	0.054	50 ± 3.7

[a]To compare the packing density of the **C18SH** SAM, the atomic concentrations of the S 2p spectra of the SAMs derived from the chelating dithiolates were divided by a factor of 2.

Table 3. Advancing (θ_a) and Receding (θ_r) Contact Angles and Hysteresis ($\Delta\theta = \theta_a - \theta_r$) for Hexadecane (HD), Water (H_2O), and Decalin (DEC) on Monolayer Films Generated from C18SH, R1ArDT, and R1ArmDT

	contact angle (deg)[a]								
	water			hexadecane			decalin		
adsorbate	θ_a	θ_r	$\Delta\theta$	θ_a	θ_r	$\Delta\theta$	θ_a	θ_r	$\Delta\theta$
C18SH	115	105	10	50	40	10	54	48	6
R1ArDT	109	99	10	45	35	10	32	27	5
R1ArmDT	109	98	11	42	32	10	31	27	4

[a]The contact angles of water, hexadecane, and decalin were reproducible within ±1°.

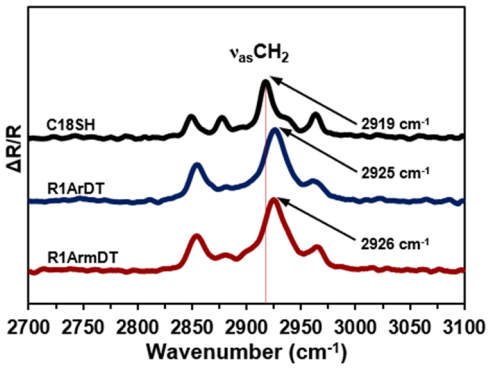

Figure 3. PM-IRRAS spectra of the C−H stretching region for the SAMs formed from **C18SH**, **R1ArDT**, and **R1ArmDT**.

Nevertheless, it is reasonable to assume that the aromatic ring in the **R1ArmDT** SAMs aligns with an upright orientation

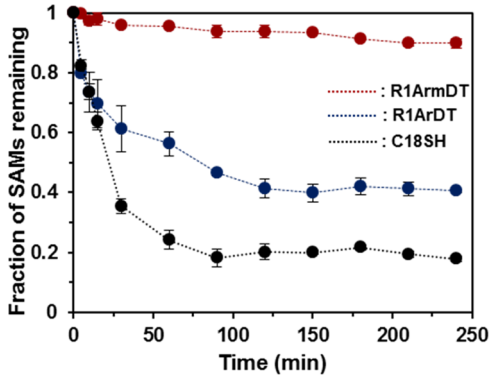

Figure 4. Relative thermal stability based upon solution-phase thermal desorption as determined by ellipsometric thickness for SAMs formed from **C18SH**, **R1ArDT**, and **R1ArmDT** in isooctane at 80 °C.

similar to the structurally analogous **R1ArDT** SAMs, where such orientation accommodates the closest packing of the aromatic adlayer and affords optimized $\pi-\pi$ stacking interactions.[38,39] When comparing the dithiolate headgroups for these two adsorbates, it is notable that **R1ArmDT** has a longer intramolecular S···S distance than that of **R1ArDT**; specifically, the calculated distances between the sulfur atoms in the dithiolate headgroups of **R1ArmDT** and **R1ArDT** are 4.90 and 3.50 Å, respectively.[40] Correspondingly, the **R1ArmDT** footprint is larger than the **R1ArDT** footprint, and **R1ArmDT** molecules would occupy a larger surface area and create a larger spacing between alkyl chains above the aromatic ring in a SAM derived from **R1ArmDT**. Consequently, to optimize the interchain van der Waals interactions, it is plausible that the long hydrocarbon chains in the **R1ArmDT** SAM would be more tilted than those in the **R1ArDT** SAM. However, given that the ellipsometric thickness of the **R1ArmDT** SAM is similar to that of the **R1ArDT** SAM (18.3 ± 0.4 Å for **R1ArmDT** vs 19.1 ± 0.3 Å for **R1ArDT**; see Table 1), we cannot draw any strong conclusions regarding differences in the relative chain tilt from the ellipsometry data. As such, we interpret these results to indicate a similar coverage and average chain tilt for both SAMs. Furthermore, the data are consistent with a model in which **R1ArmDT** adopts molecular packing densities and surface-binding sites (i.e., an overall surface organization) similar to **R1ArDT**, as discussed below in greater detail.

Packing Density of the Films. Analysis by X-ray photoelectron spectroscopy (XPS) can be used to determine

DOI: 10.1021/acs.langmuir.7b03973
Langmuir 2018, 34, 6645−6652

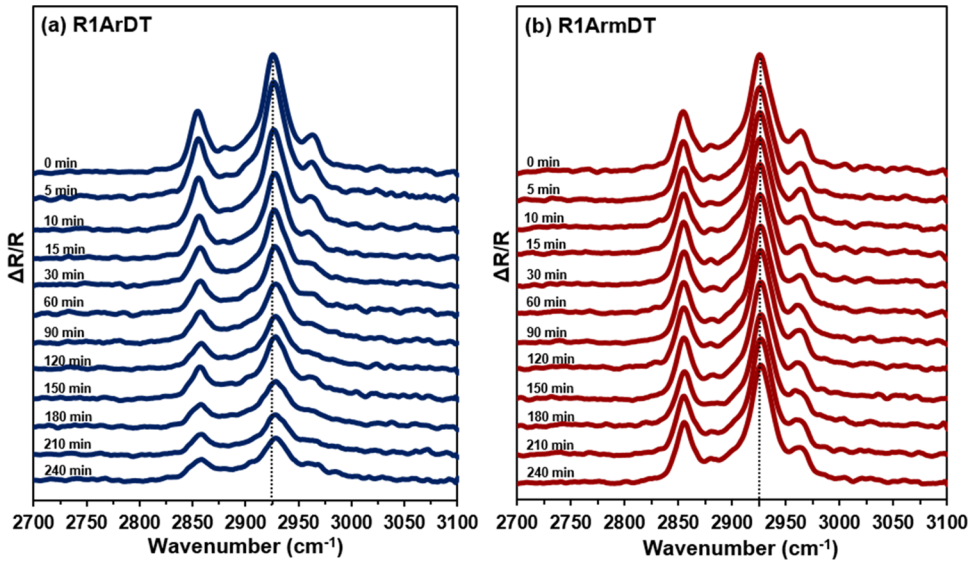

Figure 5. PM-IRRAS spectra of the C−H stretching region of the **R1ArDT** and **R1ArmDT** monolayers as a function of time heated at 80 °C in isooctane.

the chemical composition of a monolayer film as well as provide a means for calculating the relative packing density of the molecules on the surface.[41] We used XPS to evaluate the packing density of the **R1ArmDT** SAM relative to the **R1ArDT** SAM and the densely packed **C18SH** SAM as a reference. The XP spectra of the Au 4f, C 1s, S 2p, and O 1s regions for the SAMs derived from **R1ArmDT**, **R1ArDT**, and **C18SH** are shown in Figure 2. Although the spectra are consistent with the expected composition of the SAMs (based on the chemical composition of the adsorbates), we draw attention to the binding energies of the S 2p peaks, which can be used to determine whether the sulfur headgroups are fully bound to gold and/or whether any oxidized sulfur species exist in the SAMs.[42−44] For bound thiolate, the S 2p binding energy (BE) peaks appear as a 2:1 doublet at ∼162 eV (S $2p_{3/2}$) and ∼163.2 eV (S $2p_{1/2}$).[42] Additionally, the unbound and oxidized sulfur species appear at ∼163−164 eV and above 166 eV, respectively.[43,44] As shown in Figure 2c, the sulfur headgroups for all SAMs derived from **C18SH**, **R1ArDT**, and **R1ArmDT** were fully bound to gold, and there were no oxidized sulfur species in any of the SAMs. Additionally, the percentage of bound/unbound sulfur was determined by curve fitting the S 2p peaks in the X-ray photoelectron spectra as presented in Figure S5 and Table S2 in the Supporting Information. On the basis of our analysis, the percentages of bound thiolates were 99.9, 97, and 94% for **C18SH**, **R1ArDT**, and **R1ArmDT**, respectively. Therefore, our calculation of bound thiolate and the previously discussed analysis suggest that the different percentages of bound thiolates likely originate from the structural differences of the headgroups. In addition, for a reliable qualitative determination of the relative packing density of monolayer films, the binding energy of the C 1s photoelectron can be examined;[45−47] specifically, the C 1s binding energies shift to higher energy as the packing density increases, because densely packed monolayers act as good insulators. As illustrated in Figure 2b, the C 1s peak positions for the SAMs derived from **R1ArmDT**, **R1ArDT**, and **C18SH** appear at 284.7, 284.9, and 285.0 eV, respectively. According to these C 1s binding energies, the relative packing densities of the SAMs were **C18SH** > **R1ArDT** > **R1ArmDT**. These results are further consistent with a model in which the alkyl tailgroups of the SAMs derived from **R1ArDT** and **R1ArmDT** were tilted on average more than those of the SAMs derived from **C18SH**.

Additionally, the packing densities of SAMs can be obtained quantitatively from XPS by comparing the sulfur-to-gold (S/Au) ratios.[48] In the analysis here, the atomic concentrations of the S 2p spectra obtained by XPS for the **R1ArDT** and **R1ArmDT** films are divided by a factor of two compared to those of the **C18SH** film (due to the differences in stoichiometry of the bidentate vs monodentate adsorbates, respectively). The resultant packing densities are shown in Table 2, assuming 100% packing density for the standard **C18SH** SAM. The slightly lower value of the surface packing density of the **R1ArmDT** SAMs compared with that of the **R1ArDT** SAMs is consistent with the ellipsometry data and also consistent with **R1ArmDT** having a larger footprint and, therefore, occupying a larger surface area than that of **R1ArDT**. Furthermore, given the shorter distance between the benzene ring and the gold surface for **R1ArmDT** versus **R1ArDT**, it is plausible that a partial contribution from π−metal interactions[37,49] during the formation of the **R1ArmDT** monolayer might induce a tilt of the ring and also contribute to an enhancement in the footprint of **R1ArmDT**. However, calculations also support the upright configuration for this headgroup on gold (more favorable by 2.5 kcal/mol than a configuration in which the aromatic ring is parallel to the surface).[50]

Although the conformation of monolayers relies on the counterbalance of several energy parameters (e.g., those based on chain−chain, π−π, and molecule−substrate interactions),[27,51] the evidence as a whole suggests that the molecular conformation of the benzene ring in the **R1ArmDT** SAM exists with an upright orientation, which affords the closest molecular packing and the strongest intermolecular interactions (π−π and interchain) rather than the parallel and highly tilted orientation, which would reduce further the surface packing density and the intermolecular interactions.[52,53] We note also that the slightly lower chain packing density for the **R1ArmDT** SAM compared to that of the **R1ArDT** SAM implies a more loosely packed tailgroup structure for the former SAM, which would lead to

DOI: 10.1021/acs.langmuir.7b03973
Langmuir 2018, 34, 6645−6652

greater wettability for the **R1ArmDT** SAM compared to that for the **R1ArDT** SAM.[46,54] This hypothesis is supported by the wettability data, which are presented below.

Wettability of the Films. Table 3 shows the wettabilities of the organic monolayer films in the present study determined by advancing contact angle (θ_a) and receding contact angle (θ_r) measurements using water (H_2O), hexadecane (HD), and decalin (DEC) as contacting liquids. For water, the advancing ($\theta_a^{H_2O}$) and receding ($\theta_r^{H_2O}$) contact angles for the **R1ArmDT** and **R1ArDT** SAMs are roughly identical and only slightly lower than those for the **C18SH** SAM. These results suggest that the interfaces of the SAMs derived from these aromatic dithiolate adsorbates are slightly less hydrophobic than that of the **C18SH** SAM. However, the interfaces of monolayers composed of hydrocarbon-terminated molecules are somewhat insensitive to polar protic probe liquids.[19] Dispersive apolar and aprotic liquids such as hexadecane are useful for detecting nanoscale differences in the conformational order and/or packing density of SAMs having hydrocarbon tailgroups.[19] Furthermore, we used decalin, with its bulky cyclic structure, to analyze the **R1ArmDT** and **R1ArDT** SAMs, given the likelihood that their tailgroups were loosely packed and amenable to intercalation by hexadecane (but less so by decalin).[54]

Loosely packed SAMs are more wettable than densely packed SAMs due to the enhanced atomic contact per unit area at the interface, arising from interactions between the probe liquids and predominantly methylene groups (loose packing) versus methyl groups (dense packing), which leads to increased dispersive interactions between the contacting liquids and the films.[46,55] Table 3 shows that the advancing contact angle of hexadecane (θ_a^{HD}) for the **R1ArmDT** SAM is 3° less than the value for the **R1ArDT** SAM, whereas the difference for decalin (θ_a^{DEC}) is only 1° (i.e., negligible); however, the values on the **C18SH** SAM are markedly higher for both dispersive contacting liquids, consistent with a model in which the bidentate SAMs expose predominantly methylene groups (loose packing), whereas the densely packed **C18SH** SAM exposes predominantly methyl groups.[46,55] Furthermore, the lower contact angle values (particularly for hexadecane) on the **R1ArmDT** SAM when compared to those on the **R1ArDT** SAM indicate that the former monolayer is more loosely packed, in which a greater number of methylene units are exposed at the interface as compared to those at the latter monolayer.

Notably, the degree of surface roughness and heterogeneity of an interface can be evaluated by the contact angle hysteresis ($\Delta\theta = \theta_a - \theta_r$).[56,57] Notably, the hysteresis data in Table 3 suggest the least roughness/heterogeneity for the **C18SH** SAM, but no substantial macroscopic interfacial differences between the **R1ArmDT** SAM and the **R1ArDT** SAM.

Analysis by PM-IRRAS. Structural and conformational information regarding organic thin films can be obtained from the C−H stretching region of surface infrared spectra.[58−60] Importantly, the peak position and bandwidth of the methylene symmetric stretching vibration ($\nu_{as}^{CH_2}$) in *n*-alkanethiol-based SAMs are sensitive to the conformational order of the hydrocarbon backbone.[59] For highly ordered monolayers derived from *n*-alkanethiols, the position of the $\nu_{as}^{CH_2}$ stretching mode appears at ~2918 cm^{-1}. On the other hand, the shifts of the $\nu_{as}^{CH_2}$ band to higher frequencies (>2918 cm^{-1}) are observed in cases for loosely packed and disordered monolayers.[55,59] For the PM-IRRAS spectra of the monolayers shown in Figure 3, the $\nu_{as}^{CH_2}$ band for the **C18SH** monolayer appears at 2919 cm^{-1}, which indicates a film that is conformationally ordered with trans-extended hydrocarbon chains.[58,59] The higher frequency $\nu_{as}^{CH_2}$ bands for the **R1ArDT** and **R1ArmDT** SAMs (~2925 and ~2926 cm^{-1}, respectively) indicate the presence of deformation and disordering of the hydrocarbon chains (gauche conformations) for these bidentate SAMs. Furthermore, the degree of conformational order decreases as follows: **C18SH** ≫ **R1ArDT** > **R1ArmDT**; these results are consistent with the data obtained above by XPS and contact angle goniometry for these SAMs.

To acquire further insight into the structure of the SAMs with regard to the orientation of the aromatic ring, we collected low-frequency vibrational spectra to examine the aromatic C−C stretching and C−H bending modes over the range of 800−1700 cm^{-1} (data not shown). Unfortunately, the intensities of these modes were below the detection limit of our instrument to prohibit further analysis, as has been reported in previous studies of SAMs on gold having aromatic headgroups.[61,62]

Thermal Stability of the C18SH, R1ArmDT, and R1ArDT SAMs in Solution. We investigated the thermal desorption of the SAMs in the nonintercalating solvent isooctane at 80 °C. Notably, in a previous study of the **R1ArDT** SAM,[33] we attributed its enhanced thermal stability to the chelate effect and the entropic disfavor of the formation of cyclic disulfides from intra- and intermolecular desorption processes. In the case of the intramolecular desorption of the **R1ArmDT** monolayer, the formation of a cyclic disulfide by reductive elimination is precluded by the intramolecular distance between the sulfur atoms and the rigidity of the aromatic ring. Moreover, intermolecular desorption as higher order disulfides is entropically disfavored. Consequently, we anticipated that **R1ArmDT** would generate SAMs that were more robust than those derived from **R1ArDT** (and markedly more robust than those derived from **C18SH**). In the studies reported here, we examined the thickness profiles and conformational order (by ellipsometry and PM-IRRAS, respectively) of the monolayers as a function of time under elevated temperature. As shown in Figure 4, ~94% of the **R1ArmDT** SAM remained after 90 min at 80 °C; in contrast, ~47% of the **R1ArDT** SAM and ~20% of the **C18SH** SAM remained under the same conditions. Furthermore, after 240 min, the fraction of the **R1ArmDT** SAM remaining was ~90%, whereas that for the **R1ArDT** SAM was ~42% and that for the **C18SH** SAM was ~20%.[33,34,47] With regard to longer incubation times in isooctane at 80 °C (data not shown), the fractions of **C18SH**, **R1ArDT**, and **R1ArmDT** SAMs remaining after 1 day were 17, 36, and 70%, respectively. Additionally, the fraction of **R1ArmDT** SAMs remaining after 2 days was 30%; otherwise, the fractions of **C18SH** and **R1ArDT** SAMs remaining after 2 days were 6 and 10%, respectively. We did not examine longer time periods.

For the bidentate SAMs, these results correspond with the conformational changes observed during the thermal desorption process as investigated by ex situ PM-IRRAS (see Figure 5). Although the **R1ArDT** SAM exhibited a loss in intensity of the $\nu_{as}^{CH_2}$ band along with an increase in bandwidth and a shift to higher frequency with increasing incubation time corresponding with the deformation and degradation of the long alkoxy chains during the desorption process,[20,63] the $\nu_{as}^{CH_2}$ band for the **R1ArmDT** SAM changed insignificantly over the course of the experimental timeframe, indicating a negligible thermal desorption of the adsorbate molecules

DOI: 10.1021/acs.langmuir.7b03973
Langmuir 2018, 34, 6645−6652

from the gold surface. Overall, the results strongly demonstrate that **R1ArmDT** generates more thermally stable monolayers than does **R1ArDT**. We attribute this difference to the inability of the **R1ArmDT** adsorbates to undergo reductive elimination as an intramolecular disulfide due to the fact that **R1ArmDT** has a longer intramolecular S···S distance than that of **R1ArDT**.

CONCLUSIONS

The aromatic-based dithiolate adsorbate **R1ArmDT** was synthesized and used to generate SAMs on gold surfaces. The SAMs derived from **R1ArmDT** were compared to those derived from structurally related **R1ArDT** and **C18SH** as a standard. All of the SAMs were characterized by using ellipsometry, XPS, contact angle goniometry, and PM-IRRAS. Comparison of film qualities for these monolayers showed that the ellipsometric thickness, conformational order, and relative packing density of the **R1ArDT** SAM were slightly higher than those of the **R1ArmDT** SAM, which can be attributed to the larger footprint of the **R1ArmDT** headgroup on the surface of gold; notably, the average S···S distance in **R1ArmDT** was calculated to be 1.6 Å greater than that in **R1ArDT**. The evaluation of the thermal stability of the monolayers in isooctane at 80 °C as a function of time revealed an enhanced thermal stability for the **R1ArmDT** SAM compared to that for the **R1ArDT** SAM. The significant difference in the resistance of the **R1ArmDT** monolayer to undergo thermal desorption can be attributed to its longer intramolecular S···S spacing, which precludes the formation of intramolecular cyclic disulfides during the desorption process.

ASSOCIATED CONTENT

Supporting Information

The Supporting Information is available free of charge on the ACS Publications website at DOI: 10.1021/acs.langmuir.7b03973.

Descriptions of the materials and synthetic procedures used for preparing **R1ArmDT** along with the corresponding ^{1}H and ^{13}C NMR spectra; X-ray photoelectron spectra (XPS) of the S 2p region of the SAMs and their deconvolution to determine the percentages of bound and unbound thiol in the SAMs; and ellipsometric constants of the bare gold substrates (PDF)

AUTHOR INFORMATION

Corresponding Author

*E-mail: trlee@uh.edu.

ORCID

T. Randall Lee: 0000-0001-9584-8861

Author Contributions

§S.R. and C.S.P. contributed equally to this study.

Notes

The authors declare no competing financial interest.

ACKNOWLEDGMENTS

The National Science Foundation (CHE-1411265 and CHE-1710561), the Robert A. Welch Foundation (E-1320), and the Texas Center for Superconductivity at the University of Houston provided generous support for this research. J.W. thanks the National Science Foundation for grant support (CHE-1751370). Support for this work was also provided by resources from the uHPC cluster managed by the University of Houston and acquired through NSF award number MRI-1531814.

REFERENCES

(1) Love, J. C.; Estroff, L. A.; Kriebel, J. K.; Nuzzo, R. G.; Whitesides, G. M. Self-Assembled Monolayers of Thiolates on Metals as a Form of Nanotechnology. *Chem. Rev.* **2005**, *105*, 1103−1170.

(2) Ulman, A. Formation and Structure of Self-Assembled Monolayers. *Chem. Rev.* **1996**, *96*, 1533−1554.

(3) Ariga, K.; Nakanishi, T.; Michinobu, T. Immobilization of Biomaterials to Nano-Assembled Films (Self-Assembled Monolayers, Langmuir-Blodgett Films, and Layer-by-Layer Assemblies) and Their Related Functions. *J. Nanosci. Nanotechnol.* **2006**, *6*, 2278−2301.

(4) Heleg-Shabtai, V.; Katz, E.; Willner, I. Assembly of Microperoxidase-11 and Co(II)-Protoporphyrin IX Reconstituted Myoglobin Monolayers on Au-Electrodes: Integrated Bioelectrocatalytic Interfaces. *J. Am. Chem. Soc.* **1997**, *119*, 8121−8122.

(5) Park, C. S.; Lee, H. J.; Jamison, A. C.; Lee, T. R. Robust Maleimide-Functionalized Gold Surfaces and Nanoparticles Generated Using Custom-Designed Bidentate Adsorbates. *Langmuir* **2016**, *32*, 7306−7315.

(6) Dulcey, C. S.; Georger, J. H.; Chen, M.-S.; McElvany, S. W.; O'Ferrall, C. E.; Benezra, V. I.; Calvert, J. M. Photochemistry and Patterning of Self-Assembled Monolayer Films Containing Aromatic Hydrocarbon Functional Groups. *Langmuir* **1996**, *12*, 1638−1650.

(7) Herzer, N.; Hoeppener, S.; Schubert, U. S. Fabrication of Patterned Silane Based Self-Assembled Monolayers by Photolithography and Surface Reactions on Silicon-Oxide Substrates. *Chem. Commun.* **2010**, *46*, 5634.

(8) Tao, N. J. Electron Transport in Molecular Junctions. *Nat. Nanotechnol.* **2006**, *1*, 173−181.

(9) Katsonis, N.; Lubomska, M.; Pollard, M.; Feringa, B.; Rudolf, P. Synthetic Light-Activated Molecular Switches and Motors on Surfaces. *Prog. Surf. Sci.* **2007**, *82*, 407−434.

(10) Sinapi, F.; Lejeune, I.; Delhalle, J.; Mekhalif, Z. Comparative Protective Abilities of Organothiols SAM Coatings Applied to Copper Dissolution in Aqueous Environments. *Electrochim. Acta* **2007**, *52*, 5182−5190.

(11) Zamborini, F. P.; Campbell, J. K.; Crooks, R. M. Spectroscopic, Voltammetric, and Electrochemical Scanning Tunneling Microscopic Study of Underpotentially Deposited Cu Corrosion and Passivation with Self-Assembled Organomercaptan Monolayers. *Langmuir* **1998**, *14*, 640−647.

(12) Cichomski, M.; Grobelny, J.; Celichowski, G. Preparation and Tribological Tests of Thin Fluoroorganic Films. *Appl. Surf. Sci.* **2008**, *254*, 4273−4278.

(13) Shon, Y.-S.; Lee, T. R. Desorption and Exchange of Self-Assembled Monolayers (SAMs) on Gold Generated from Chelating Alkanedithiols. *J. Phys. Chem. B* **2000**, *104*, 8192−8200.

(14) Vaidya, R.; Simonson, R. J.; Cesarano, J.; Dimos, D.; López, G. P. Formation and Stability of Self-Assembled Monolayers on Thin Films of Lead Zirconate Titanate (PZT). *Langmuir* **1996**, *12*, 2830−2836.

(15) Wang, M.; Comrie, J. E.; Bai, Y.; He, X.; Guo, S.; Huck, W. T. S. Formation of Hierarchically Structured Thin Films. *Adv. Funct. Mater.* **2009**, *19*, 2236−2243.

(16) Zhou, C.; Trionfi, A.; Jones, J. C.; Hsu, J. W. P.; Walker, A. V. Comparison of Chemical Lithography Using Alkanethiolate Self-Assembled Monolayers on GaAs (001) and Au. *Langmuir* **2010**, *26*, 4523−4528.

(17) Ballav, N.; Schilp, S.; Zharnikov, M. Electron-Beam Chemical Lithography with Aliphatic Self-Assembled Monolayers. *Angew. Chem., Int. Ed.* **2008**, *47*, 1421−1424.

(18) Willey, T. M.; Vance, A. L.; van Buuren, T.; Bostedt, C.; Terminello, L. J.; Fadley, C. S. Rapid Degradation of Alkanethiol-Based Self-Assembled Monolayers on Gold in Ambient Laboratory Conditions. *Surf. Sci.* **2005**, *576*, 188−196.

(19) Bain, C. D.; Troughton, E. B.; Tao, Y. T.; Evall, J.; Whitesides, G. M.; Nuzzo, R. G. Formation of Monolayer Films by the

DOI: 10.1021/acs.langmuir.7b03973
Langmuir 2018, 34, 6645−6652

Spontaneous Assembly of Organic Thiols from Solution onto Gold. *J. Am. Chem. Soc.* **1989**, *111*, 321−335.
(20) Bensebaa, F.; Ellis, T. H.; Badia, A.; Lennox, R. B. Thermal Treatment of *n*-Alkanethiolate Monolayers on Gold, As Observed by Infrared Spectroscopy. *Langmuir* **1998**, *14*, 2361−2367.
(21) Widrig, C. A.; Chung, C.; Porter, M. D. The Electrochemical Desorption of *n*-Alkanethiol Monolayers from Polycrystalline Au and Ag Electrodes. *J. Electroanal. Chem. Interfacial Electrochem.* **1991**, *310*, 335−359.
(22) Kondoh, H.; Kodama, C.; Sumida, H.; Nozoye, H. Molecular Processes of Adsorption and Desorption of Alkanethiol Monolayers on Au(111). *J. Chem. Phys.* **1999**, *111*, 1175−1184.
(23) Jennings, G. K.; Laibinis, P. E. Self-Assembled *n*-Alkanethiolate Monolayers on Underpotentially Deposited Adlayers of Silver and Copper on Gold. *J. Am. Chem. Soc.* **1997**, *119*, 5208−5214.
(24) Kim, T.; Chan, K. C.; Crooks, R. M. Polymeric Self-Assembled Monolayers. 4. Chemical, Electrochemical, and Thermal Stability of ω-Functionalized, Self-Assembled Diacetylenic and Polydiacetylenic Monolayers. *J. Am. Chem. Soc.* **1997**, *119*, 189−193.
(25) Srisombat, L.; Jamison, A. C.; Lee, T. R. Stability: A Key Issue for Self-Assembled Monolayers on Gold as Thin-Film Coatings and Nanoparticle Protectants. *Colloids Surf., A* **2011**, *390*, 1−19.
(26) Garg, N.; Lee, T. R. Self-Assembled Monolayers Based on Chelating Aromatic Dithiols on Gold. *Langmuir* **1998**, *14*, 3815−3819.
(27) Kühnle, A. Self-Assembly of Organic Molecules at Metal Surfaces. *Curr. Opin. Colloid Interface Sci.* **2009**, *14*, 157−168.
(28) Lee, H. J.; Jamison, A. C.; Lee, T. R. Boc-Protected ω-Amino Alkanedithiols Provide Chemically and Thermally Stable Amine-Terminated Monolayers on Gold. *Langmuir* **2015**, *31*, 2136−2146.
(29) Park, C. S.; Lee, H. J.; Jamison, A. C.; Lee, T. R. Robust Thick Polymer Brushes Grafted from Gold Surfaces Using Bidentate Thiol-Based Atom-Transfer Radical Polymerization Initiators. *ACS Appl. Mater. Interfaces* **2016**, *8*, 5586−5594.
(30) Lee, H. J.; Jamison, A. C.; Lee, T. R. Entropy-Driven Conformational Control of α,ω-Difunctional Bidentate-Dithiol Azo-Based Adsorbates Enables the Fabrication of Thermally Stable Surface-Grafted Polymer Films. *ACS Appl. Mater. Interfaces* **2016**, *8*, 15691−15699.
(31) Schlenoff, J. B.; Li, M.; Ly, H. Stability and Self-Exchange in Alkanethiol Monolayers. *J. Am. Chem. Soc.* **1995**, *117*, 12528−12536.
(32) Bruno, G.; Babudri, F.; Operamolla, A.; Bianco, G. V.; Losurdo, M.; Giangregorio, M. M.; Omar, O. H.; Mavelli, F.; Farinola, G. M.; Capezzuto, P.; Naso, F. Tailoring Density and Optical and Thermal Behavior of Gold Surfaces and Nanoparticles Exploiting Aromatic Dithiols. *Langmuir* **2010**, *26*, 8430−8440.
(33) Rittikulsittichai, S.; Park, C. S.; Jamison, A. C.; Rodriguez, D.; Zenasni, O.; Lee, T. R. Bidentate Aromatic Thiols on Gold: New Insight Regarding the Influence of Branching on the Structure, Packing, Wetting, and Stability of Self-Assembled Monolayers on Gold Surfaces. *Langmuir* **2017**, *33*, 4396−4406.
(34) Lim, J. K.; Kim, Y.; Kwon, O.; Joo, S.-W. Adsorption of 1,3-Benzenedithiol and 1,3-Benzenedimethanethiol on Gold Surfaces. *ChemPhysChem* **2008**, *9*, 1781−1787.
(35) Fenter, P.; Eberhardt, A.; Liang, K. S.; Eisenberger, P. Epitaxy and Chainlength Dependent Strain in Self-Assembled Monolayers. *J. Chem. Phys.* **1997**, *106*, 1600−1608.
(36) Evans, S. D.; Urankar, E.; Ulman, A.; Ferris, N. Self-Assembled Monolayers of Alkanethiols Containing a Polar Aromatic Group: Effects of the Dipole Position on Molecular Packing, Orientation, and Surface Wetting Properties. *J. Am. Chem. Soc.* **1991**, *113*, 4121−4131.
(37) Chang, S.-C.; Chao, I.; Tao, Y.-T. Structure of Self-Assembled Monolayers of Aromatic-Derivatized Thiols on Evaporated Gold and Silver Surfaces: Implication on Packing Mechanism. *J. Am. Chem. Soc.* **1994**, *116*, 6792−6805.
(38) Dou, R. F.; Ma, X. C.; Xi, L.; Yip, H. L.; Wong, K. Y.; Lau, W. M.; Jia, J. F.; Xue, Q. K.; Yang, W. S.; Ma, H.; Jen, A. K. Y. Self-Assembled Monolayers of Aromatic Thiols Stabilized by Parallel-Displaced π-π Stacking Interactions. *Langmuir* **2006**, *22*, 3049−3056.
(39) Skibinski, E. S.; Song, A.; DeBenedetti, W. J. I.; Ortoll-Bloch, A. G.; Hines, M. A. Solution Deposition of Self-Assembled Benzoate Monolayers on Rutile (110): Effect of π−π Interactions on Monolayer Structure. *J. Phys. Chem. C* **2016**, *120*, 11581−11589.
(40) The quantum mechanical computations were performed for the headgroups of R1ArmDT and R1ArDT using Gaussian 09, Revision D.01. The density functional theory ωB97XD paired with basis sets 6-311+G(d,p) was employed in the geometry optimization. For R1ArmDT, the Cs symmetry was enforced during the optimization to keep the thiol group in the *cis* conformation.
(41) Laibinis, P. E.; Whitesides, G. M.; Allara, D. L.; Tao, Y. T.; Parikh, A. N.; Nuzzo, R. G. Comparison of the Structures and Wetting Properties of Self-Assembled Monolayers of *n*-Alkanethiols on the Coinage Metal Surfaces, Copper, Silver, and Gold. *J. Am. Chem. Soc.* **1991**, *113*, 7152−7167.
(42) Castner, D. G.; Hinds, K.; Grainger, D. W. X-Ray Photoelectron Spectroscopy Sulfur 2p Study of Organic Thiol and Disulfide Binding Interactions with Gold Surfaces. *Langmuir* **1996**, *12*, 5083−5086.
(43) Heeg, J.; Schubert, U.; Küchenmeister, F. Mixed Self-Assembled Monolayers of Terminally Functionalized Thiols at Gold Surfaces Characterized by Angle Resolved X-Ray Photoelectron Spectroscopy (ARXPS) Studies. *Fresenius J. Anal. Chem.* **1999**, *365*, 272−276.
(44) Hutt, D. A.; Leggett, G. J. Influence of Adsorbate Ordering on Rates of UV Photooxidation of Self-Assembled Monolayers. *J. Phys. Chem.* **1996**, *100*, 6657−6662.
(45) Ishida, T.; Hara, M.; Kojima, I.; Tsuneda, S.; Nishida, N.; Sasabe, H.; Knoll, W. High Resolution X-Ray Photoelectron Spectroscopy Measurements of Octadecanethiol Self-Assembled Monolayers on Au(111). *Langmuir* **1998**, *14*, 2092−2096.
(46) Park, J.-S.; Smith, A. C.; Lee, T. R. Loosely Packed Self-Assembled Monolayers on Gold Generated from 2-Alkyl-2-Methyl-propane-1,3-Dithiols. *Langmuir* **2004**, *20*, 5829−5836.
(47) Yang, Y. W.; Fan, L. J. High-Resolution XPS Study of Decanethiol on Au(111): Single Sulfur−Gold Bonding Interaction. *Langmuir* **2002**, *18*, 1157−1164.
(48) Shon, Y.-S.; Colorado, R.; Williams, C. T.; Bain, C. D.; Lee, T. R. Low-Density Self-Assembled Monolayers on Gold Derived from Chelating 2-Monoalkylpropane-1,3-Dithiols. *Langmuir* **2000**, *16*, 541−548.
(49) Murty, K. V. G. K.; Venkataramanan, M.; Pradeep, T. Self-Assembled Monolayers of 1,4-Benzenedimethanethiol on Polycrystalline Silver and Gold Films: An Investigation of Structure, Stability, Dynamics, and Reactivity. *Langmuir* **1998**, *14*, 5446−5456.
(50) Bruno, G.; Babudri, F.; Operamolla, A.; Bianco, G. V.; Losurdo, M.; Giangregorio, M. M.; Hassan Omar, O.; Mavelli, F.; Farinola, G. M.; Capezzuto, P.; Naso, F. Tailoring Density and Optical and Thermal Behavior of Gold Surfaces and Nanoparticles Exploiting Aromatic Dithiols. *Langmuir* **2010**, *26*, 8430−8440.
(51) Sellers, H.; Ulman, A.; Shnidman, Y.; Eilers, J. E. Structure and Binding of Alkanethiolates on Gold and Silver Surfaces: Implications for Self-Assembled Monolayers. *J. Am. Chem. Soc.* **1993**, *115*, 9389−9401.
(52) Kim, C. H.; Han, S. W.; Ha, T. H.; Kim, K. *O*-Xylene-α,α′-Dithiol Monolayer Film on Gold: Fourier Transform Infrared Spectroscopy, Quartz Crystal Microbalance, and Atomic Force Microscopy Study. *Langmuir* **1999**, *15*, 8399−8404.
(53) Tao, Y.-T.; Wu, C.-C.; Eu, J.-Y.; Lin, W.-L.; Wu, K.-C.; Chen, C. Structure Evolution of Aromatic-Derivatized Thiol Monolayers on Evaporated Gold. *Langmuir* **1997**, *13*, 4018−4023.
(54) Park, J.-S.; Vo, A. N.; Barriet, D.; Shon, Y.-S.; Lee, T. R. Systematic Control of the Packing Density of Self-Assembled Monolayers Using Bidentate and Tridentate Chelating Alkanethiols. *Langmuir* **2005**, *21*, 2902−2911.
(55) Shon, Y.-S.; Lee, S.; Colorado, R.; Perry, S. S.; Lee, T. R. Spiroalkanedithiol-Based SAMs Reveal Unique Insight into the Wettabilities and Frictional Properties of Organic Thin Films. *J. Am. Chem. Soc.* **2000**, *122*, 7556−7563.

DOI: 10.1021/acs.langmuir.7b03973
Langmuir 2018, 34, 6645−6652

(56) Wang, X. D.; Peng, X. F.; Lu, J. F.; Liu, T.; Wang, B. X. Contact Angle Hysteresis on Rough Solid Surfaces. *Heat Transfer − Asian Res.* **2004**, *33*, 201−210.
(57) Extrand, C. W. Contact Angles and Hysteresis on Surfaces with Chemically Heterogeneous Islands. *Langmuir* **2003**, *19*, 3793−3796.
(58) Snyder, R. G.; Strauss, H. L.; Elliger, C. A. Carbon-Hydrogen Stretching Modes and the Structure of *n*-Alkyl Chains. 1. Long, Disordered Chains. *J. Phys. Chem.* **1982**, *86*, 5145−5150.
(59) Porter, M. D.; Bright, T. B.; Allara, D. L.; Chidsey, C. E. D. Spontaneously Organized Molecular Assemblies. 4. Structural Characterization of *n*-Alkyl Thiol Monolayers on Gold by Optical Ellipsometry, Infrared Spectroscopy, and Electrochemistry. *J. Am. Chem. Soc.* **1987**, *109*, 3559−3568.
(60) MacPhail, R. A.; Strauss, H. L.; Snyder, R. G.; Elliger, C. A. Carbon-Hydrogen Stretching Modes and the Structure of *n*-Alkyl Chains. 2. Long, All-Trans Chains. *J. Phys. Chem.* **1984**, *88*, 334−341.
(61) Lee, S. H.; Puck, A.; Graupe, M.; Colorado, R.; Shon, Y.-S.; Lee, T. R.; Perry, S. S. Structure, Wettability, and Frictional Properties of Phenyl-Terminated Self-Assembled Monolayers on Gold. *Langmuir* **2001**, *17*, 7364−7370.
(62) Rittikulsittichai, S.; Jamison, A. C.; Lee, T. R. Self-Assembled Monolayers Derived from Alkoxyphenylethanethiols Having One, Two, and Three Pendant Chains. *Langmuir* **2011**, *27*, 9920−9927.
(63) Bensebaa, F.; Ellis, T. H.; Badia, A.; Lennox, R. B. Probing the Different Phases of Self-Assembled Monolayers on Metal Surfaces: Temperature Dependence of the C−H Stretching Modes. *J. Vac. Sci. Technol., A* **1995**, *13*, 1331−1336.

DOI: 10.1021/acs.langmuir.7b03973
Langmuir 2018, 34, 6645−6652